PHILOSOPHICAL TRANSACTIONS OF THE ROYAL SOCIETY B BIOLOGICAL SCIENCES

On Pattern Formation Mechanisms for Lepidopteran Wing Patterns and Mammalian Coat Markings

J. D. Murray

Phil. Trans. R. Soc. Lond. B 1981 **295**, 473-496
doi: 10.1098/rstb.1981.0155

Phil. Trans. R. Soc. Lond. B **295**, 473–496 (1981)
Printed in Great Britain

On pattern formation mechanisms for lepidopteran wing patterns and mammalian coat markings

By J. D. Murray

University of Oxford, Mathematical Institute,
24–29 St Giles, Oxford OX1 3LB, U.K.

The patterns on wings of Lepidoptera can be generated with a few pattern elements, but no mechanism has been suggested for producing them. I consider two of the basic patterns, namely, central symmetry and dependent patterns. A biochemically plausible model mechanism is proposed for generating major aspects of these patterns, based on a diffusing morphogen that activates a gene or colour-specific enzyme in a threshold manner to generate a stable heterogeneous spatial pattern. The model is applied to the determination stream hypothesis of Kühn & von Engelhardt (*Wilhelm Roux Arch. EntwMech. Org.* **130**, 660 (1933)), and results from the model compared with their microcautery experiments on the pupal wing of *Ephestia kühniella*. In the case of dependent patterns, results are compared with patterns on specific Papilionidae. For the same mechanism and a fixed set of parameters I demonstrate the important roles of geometry and scale on the spatial patterns obtained. The results and evidence presented here suggest the existence of diffusion fields of the order of several millimetres, which are very much larger than most embryonic fields. The existence of zones of polarizing activity is also indicated.

Colour patterns on animals are considered to be genetically determined, but the mechanism is not known. I have previously suggested that a single mechanism that can exhibit an infinite variety of patterns is a candidate for that mechanism, and proposed that a reaction–diffusion system that can be diffusively driven unstable could be responsible for the laying down of the spacing patterns that generates the prepattern for animal coat markings.

For illustrative purposes I consider a practical reaction mechanism, which exhibits substrate inhibition, and show that the geometry and scale of the domain (part of the epidermis) play a crucial role in the structural patterns that result. Patterns are obtained for a selection of geometries, and general features are related to the coat colour distribution in the spotted Felidae, giraffe, zebra and other animals. The patterns depend on the initial conditions, but for a given geometry and scale are *qualitatively* similar, a positive feature of the model and a necessary model attribute in view of the pattern individuality on animals of the same species.

1. Introduction and background

The development of pattern is naturally of consuming interest in developmental biology. Most experimental studies of biological pattern formation and model mechanisms for them have been concerned with early patterns in the ontogeny of complex organisms or with regeneration. The phenomenological positional information approach (Wolpert 1971) and later work on the chick limb based on it (see, for example, Summerbell & Tickle 1977; Wolpert & Hornchurch 1981; Smith & Wolpert 1981; also further references therein) and the regulatory intercalation model (French *et al.* 1976) are major examples. Meinhardt (1978) reviews several of the many model mechanisms that have been studied.

Although the development of the colour pattern on the integument of mammals and wings of butterflies and moths occurs towards the end of morphogenesis, it reflects an underlying pre-pattern that is laid down much earlier. With mammalian markings the pre-pattern is almost certainly laid down in the very early stages of embryonic development (in the first few weeks) while that of lepidopteran wing patterns mainly during the early pupal stage or in some cases just before it (Nijhout 1980*b*).

No specific mechanism has yet been proposed for the pattern formation on wings. However, in mammalian coat markings a universal reaction–diffusion mechanism has been suggested for pre-pattern formation (Murray 1979, 1981).

In this paper I propose a primitive model mechanism for wing patterns that involves a diffusing morphogen and a biochemically plausible gene or colour-specific enzyme activation switch process for generating some frequently occurring pattern elements in lepidopteran wings. It is applied to various experiments concerned with the effect of cautery on wing patterns and the determination stream hypothesis (Kühn & von Engelhardt 1933). I also describe briefly the proposed mechanism for mammalian coat markings (Murray 1979, 1981) and present some general and further results on patterns obtained, and compare them with those found on specific animals like the Felidae, zebra and giraffe. A major feature of these model mechanisms (and any pattern formation mechanism) is the critical dependence of pattern on the geometry and scale of the integument. In the mechanism for mammalian coat patterns I suggest that they are possibly the most important factors in their determination. At first sight the diversity of mammalian patterns might appear to indicate that several mechanisms are required: I show here that this is not necessarily so.

The study of butterfly colours and wing patterns has a long history. A major survey of the field at the end of the nineteenth century is given by Mayer (1897). The extensive work on wing patterns carried out since 1920, mainly between 1924 and 1948, and associated with, for example, Henke (1928, 1933, 1943, 1948), Kühn (1926, 1936; Kühn & von Engelhardt 1933), Süffert (1927, 1929), Schwantwitsch (1924, 1925, 1929, 1935) and their coworkers is reviewed by Sondhi (1963). A succinct and definite review of the major elements in lepidopteran wing patterns is given by Nijhout (1978). Recently, on the basis of a large number of experiments, Sibatani (1980) has surveyed wing homoeosis in Lepidoptera.

The formation of the wide variety of pattern found on wings has been shown (Süffert, 1925, 1927, 1929) to be made up of relatively few pattern elements. Of these, central symmetry patterns are common, particularly so in moth wings, and at their simplest consist of approximately mirror image patterns about a central anterior–posterior axis across the middle of the wing. They were studied extensively (Kühn & von Engelhardt 1933) in an attempt to understand the pattern formation in the wings of *Ephestia kühniella*. They proposed a phenomenological model in which a 'determination stream' emanates from sources at the anterior and posterior edges of the wing and progresses as a wave across the wing to produce anterior–posterior bands of pigment (see figure 1*b*). They carried out microcautery experiments on the pupal wing; the results support their hypothesis. Work by Henke (1948) on 'spreading fields' in *Lymantria dispar* also supports this hypothesis. Results from the model mechanism in this paper are compared with these experiments in § 3 below. The model relies on scale-forming stem cells in the epithelium reacting to the underlying patterns laid down during the pupal or just pre-pupal stage. Goldschmidt (1920) suggested that primary patterns may be laid down before the pattern is seen: accumulated evidence since then seems to confirm this.

PHILOSOPHICAL TRANSACTIONS OF THE ROYAL SOCIETY B BIOLOGICAL SCIENCES

Occeli are important elements in many butterfly wings and pose a challenging pattern formation problem. Seminal work in this area has been done by Nijhout (1978, 1980*a*, *b*). Nijhout (1978) postulates a gradient model based on a conical distribution with the apex as the reference point for positional information: the apex is considered to be the focus of the occelus. Nijhout (1980*a*) presents evidence, from experiments on the nymphalid butterfly *Precis coenia*, that the foci are the influencing factors in surrounding pattern formation. The foci generate a morphogen the level of which activates a colour-specific enzyme. Melanogenesis in *Precis coenia* involves melanins (Nijhout 1980*b*) not all produced at the same time. Sibatani (1980) proposes an alternative model based on the existence of an underlying pre-pattern and suggests that the occelus-forming process involves several interacting variables. These two models are not necessarily mutually exclusive since a positional information model relies on cells reacting in a specified manner to the concentration level of some chemical: this could involve, in Nijhout's (1978) model, the morphogen generated at the occelus eye reacting to an underlying pattern. It is possible that if a model *mechanism* could be found which can generate occeli patterns then the variety of effects on occeli that span wing 'cells' (regions on the wing bounded by veins and wing edge: see figure 1*a*) could be inferred. Also, the existence of underlying pre-patterns could perhaps be determined.

The cautery work of Kühn & von Engelhardt (1933) suggests that there are at least two mechanisms in the pattern formation in *Ephestia kühniella*, since different effects are obtained depending on the time after pupation that the cauterization is done. There are probably several independent pattern-formation systems operating, as was suggested by Schwantwitsch (1924) and Süffert (1925, 1927). However, the same mechanism, such as that discussed in this paper, could be operating at different times, which could imply different parameter values and different geometries and scale to produce quite different patterns. Possibly the number of melanins present indicates the minimum number of mechanisms.

One reason for studying wing pattern in Lepidoptera is to try to understand them with a view to finding a pattern formation mechanism (or mechanisms) that produces them. Such a model mechanism must involve differentiation in time and space. Another reason is to present evidence, admittedly circumstantial, for the existence of diffusion fields greater than about 100 cells, which is about the maximum found so far: here I believe that fields of the order of 5 mm exist. From a modelling point of view an interesting aspect is that the evolution of pattern is essentially two-dimensional, which necessitates an understanding of the roles of geometry and scale. I thus wish to demonstrate the seemingly different patterns that can be generated with the same mechanism simply by its activation at different times on different geometries or scale, or both.

In § 2 I describe my model mechanisms with the mathematical details given in the appendix, and show how a simple spatial pattern can be generated with central symmetry and dependent patterns in mind. In § 3 I present some numerical solutions from my model for central symmetry patterns and compare relevant cases with experiment, particularly on *Ephestia*: there is encouraging qualitative agreement. With dependent patterns, which are particularly prevalent in Papilionidae and nymphalid butterflies, I present some computed solutions from this mechanism and compare them with known facts and typical members of a large class of butterflies that exhibit marked dependent patterns.

Mammalian coloration is due to melanin in the epidermis. The melanin is present in pigment cells (melanocytes), which derive from embryonic neural crest material. Epidermal distribution

PHILOSOPHICAL TRANSACTIONS OF THE ROYAL SOCIETY B BIOLOGICAL SCIENCES

of melanocytes is not uniform. Graft experiments indicate that melanogenesis is related to the availability of some substrate. The essentials of melanogenesis are given by the Raper–Mason theory (see Nicolaus 1968) in which tyrosine, a precursor of melanin, is oxidized to DOPA in the presence of the enzyme tyrosinase. Further oxidations result in melanin.

Few detailed experimental studies have been made on epidermal patterns in vertebrates. Notable exceptions are those with chimeric mice, a definitive survey and review of which are given in the book by McLaren (1976).

Searle (1968), in his book on comparative genetics of animal coloration, hypothesized that a reaction–diffusion mechanism might be appropriate for pattern formation. For zebra, Bard (1977) proposed that a single mechanism, as yet unknown, is responsible for the stripe pattern.

For illustrative purposes I consider a substrate inhibition reaction mechanism studied experimentally by Thomas (1976) and discuss some of the patterns that can be obtained by a Turing (1952) type of diffusion driven instability. In particular I demonstrate their critical dependence on geometry and scale. General and recurring characteristics are shown to be closely related to those in various animal coat patterns. A pedagogical discussion of some practical applications of reaction–diffusion systems in general is given in Murray (1977).

I have discussed fully (Murray 1979, 1981) the model mechanism described here, the diffusion-driven instabilities that result in steady-state spatial patterns and the application to a variety of mammalian markings. (This reaction–diffusion mechanism has also been studied by Bunow *et al.* (1980), considering *Drosophila* wing compartments.) I suggested that a reaction–diffusion mechanism could be responsible for most of the coloration patterns on animals. That a single mechanism could suffice has also been suggested by G. H. Findlay (personal communication 1979) from his work with zebra and giraffe. In § 4 I briefly describe the model, give some further results for a variety of geometries and compare them with the typical markings on specific animals to substantiate my hypothesis; details and the mathematical analysis are given elsewhere (Murray 1981).

2. Model mechanism for central symmetry and dependent patterns on lepidopteran wings: diffusing-morphogen–gene-activation system

Crossbands of pigment running generally from the anterior to the posterior of wings of butterflies and moths are possibly the most prevalent. Dislocation of these bands along wing cells, that is regions bounded by veins and a wing edge, can give rise to a remarkably wide variety of patterns (see, for example, Schwantwitsch 1925, 1929; Süffert 1927, 1929; Nijhout 1978). Figure 1 *a* is a diagram of a forewing of a generalized lepidopteran, and illustrates typical venation including those in the discal cell (D), which later atrophy. The commonest manifestation of crossbands is when they are arranged more or less symmetrically about a central axis, running down the middle of the wing from the anterior to posterior: this is the central symmetry system. Kühn & von Engelhardt (1933) carried out an extensive series of experiments, using microcautery at the pupal stage, to try to understand how such central symmetry patterns arose on the forewing of the moth *Ephestia kühniella*. Some of their results are illustrated in figure 4 *a–c* and seem consistent with the suggestion that a 'determination stream' is generated by sources on the anterior and posterior edges of the wing (like zones of polarizing activity in fact), namely at A and P in figure 1 *b*. The front of this 'stream' is associated with the position of the crossbands

of the central symmetry system. The work of Schwartz (1962) on another moth tends to confirm the existence of a determination stream for central symmetry systems. Experiments on such streams and the related 'spreading fields' of Henke (1948) are reviewed by Sondhi (1963) and Nijhout (1978). To date, it seems that neither the origin nor a mechanism that could produce them has been found. Here I propose a possible biochemically plausible model mechanism and compare results from it with those from experiment.

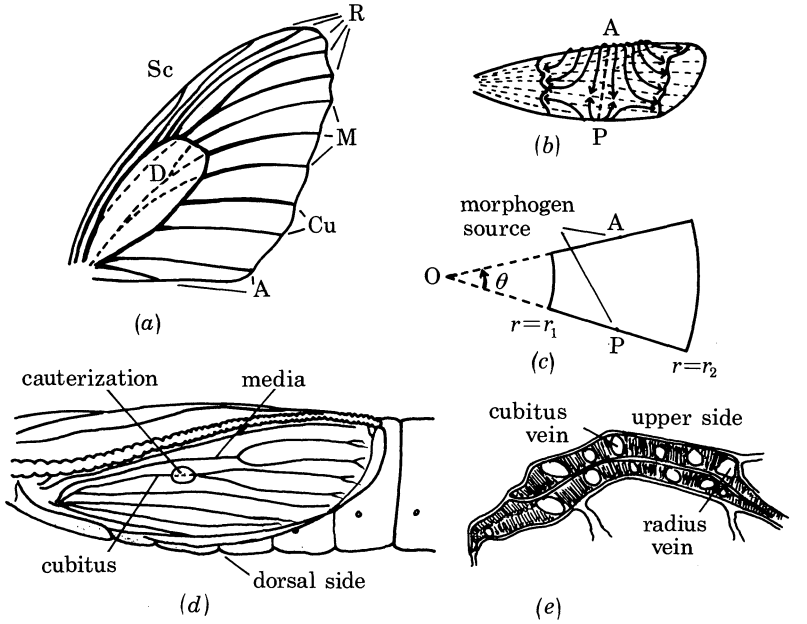

FIGURE 1. (*a*) Forewing of a generalized lepidopteran with venation: A, anal; Cu, cubitus; M, media; R, radius; Sc, subcosta; D, discal. Regions between veins are wing cells. Dotted lines represent veins that exist at the pupal stage, but later atrophy. (*b*) Hypothesized 'determination stream' for central symmetry pattern formation (after Kühn & von Engelhardt 1933). (*c*) Idealized pupal wing with A and P the anterior and posterior sources of the determination stream (morphogen). (*d*) Schematic representation of the right pupa wing approximately 6–12 h old (after Kühn & von Engelhardt 1933). (*e*) Schematic cross section through the wing vertically through the cauterized region, showing the upper and lower epithelia and veins (after Kühn & von Engelhardt 1933).

From the experimental work on *Ephestia kühniella* (Kühn & von Engelhardt 1933), *Plodia interpunctella* (Schwartz 1962) and *Malacosoma americana* (Nijhout 1978) it appears that the critical period for laying down their central symmetry pattern is in the first 1–2 days after pupation. The effect of microcautery after this period is different to that during it (Kühn & von Engelhardt 1933), hence the implication of more than one mechanism. The model that I propose is for the earlier period, namely just after pupation.

In my primitive model we have sources of a morphogen S situated at A and P on the anterior and posterior edges of the wing, which for simplicity (not necessity) in the numerical calculations I idealize as shown in figure 1*c* to be a circular sector of angle θ and radius r_1 and r_2. At a given time, genetically determined, in the pupal stage a given amount of morphogen is released and it diffuses across the wing. The wing has an upper and lower epithelial surface layer of cells and vein distribution such as illustrated in figure 1*d*, *e*. The pattern on the upper and lower sides of the wing are determined independently. As the morphogen diffuses it is also degraded in proportion to its local concentration. The diffusion field is the wing surface and so we have zero

PHILOSOPHICAL TRANSACTIONS OF THE ROYAL SOCIETY B BIOLOGICAL SCIENCES

flux boundary conditions for the morphogen at the wing edges. The governing equation for the morphogen concentration S, which is a function of the space variables r, θ and time t is then

$$\frac{\partial S}{\partial t} = D\left(\frac{\partial^2 S}{\partial r^2} + \frac{1}{r}\frac{\partial S}{\partial \theta} + \frac{1}{r^2}\frac{\partial^2 S}{\partial \theta^2}\right) - \gamma K S, \tag{1}$$

i.e. (rate of change of S with time) = (diffusion of S) – (degradation proportional to S), where $D/(\mathrm{cm^2\,s^{-1}})$ is the diffusion coefficient and $K/\mathrm{s^{-1}}$ the degradation rate constant. The parameter γ is a scale parameter (see the appendix, where the non-dimensional model system is derived). It could be incorporated into the K but I retain it in this form since it can be varied to represent change of scale. With l/cm the reference length of a 'standard wing' (for example, that studied by Kühn & von Engelhardt (1933)) and a/cm the corresponding length in a similar wing, $\gamma = a^2/l^2$, a dimensionless number. Thus if we fix D, K and the geometry we can represent the results for similar wings by a figure of the *same* size but with different γ. For example $\gamma = 4$ represents a similar wing to that with $\gamma = 1$ but with linear dimensions twice that with $\gamma = 1$.

A value for K at this stage would be purely speculative: it is probably species dependent. A typical value for the diffusion coefficients D of the morphogen through cells is possibly of the order of $2.7 \times 10^{-7}\,\mathrm{cm^2\,s^{-1}}$ (Crick 1970). Depending on the morphogen, and the fact that the diffusion domain is quasi-two-dimensional, it could be larger. In their experimental work on hair morphogenesis in *Acetabularia* (Harrison *et al.* 1980), a diffusion coefficient of the order $10^{-5}\,\mathrm{cm^2\,s^{-1}}$ was suggested. They considered a reaction–diffusion model for the hair spacing and showed that the change in diffusion coefficient with temperature was reflected, as indicated by their model, with hair spacing variation with temperature that they found experimentally.

Typical lengths envisaged for the diffusion field in my mechanism are of the order of several millimetres, which is much larger than most embryonic fields. With L/cm a typical length of interest, the diffusion time T to cover a distance L is of the order of L^2/D. If pattern formation takes place in the order of 1–2 days and say $L \approx 5$ mm, a diffusion coefficient of the order of $1\text{–}2 \times 10^{-6}\,\mathrm{cm^2\,s^{-1}}$ would be required. This is not unreasonable, in fact, since mean diffusion times in two and three dimensions can be quite different (Murray 1977). Consistent with a diffusion process is the change, with temperature, in the mean rate at which eyespot determination spreads across the wing (by a comparable mechanism perhaps): Nijhout (1980*a*) found it to be 0.27 mm/day at 29 °C and 0.12 mm/day at 19 °C.

As S diffuses across the wing surface, let us consider the cells to react in response to the local morphogen level, and a gene G to be activated by S to produce a product g and the kinetics of the gene product to exhibit a biochemical switch behaviour: see figure 2. Such a mechanism can effect a permanent change in the gene product level. Alternatively, a model, with similar kinetics, in which the morphogen activates a colour-specific enzyme that depends on the local morphogen level is also a possible mechanism. There are now many such biochemically plausible switch mechanisms (see, for example, Edelstein 1972; Babloyantz & Hiernaux 1975). Although it is not qualitatively critical which mechanism we use, to be specific let us consider here that proposed by G. Mitchison and used by Lewis *et al.* (1977). Here the gene product is activated linearly by the morphogen S, by its own product in a nonlinear positive feedback way and linearly degraded proportional to itself. The governing equation for g, the concentration of g, is (see also the appendix)

$$\mathrm{d}g/\mathrm{d}t = \gamma(k_1 S + k_2 g^2/(1+g^2) - k_3 g), \tag{2}$$

PHILOSOPHICAL TRANSACTIONS OF THE ROYAL SOCIETY B BIOLOGICAL SCIENCES

i.e. (rate of change of gene product with time) = (linear activation by the morphogen) + (self-activation with positive feedback control) − (linear degradation), where as before γ is the scale factor described above, and k_1, k_2 and k_3 are positive constants. The product g is a function of space (through S) and of time.

The threshold and switch properties of the mechanism (2) can be seen by considering the schematic graph of $\gamma^{-1}\mathrm{d}g/\mathrm{d}t$ as a function of g, as in figure 2*a*, for various S. If k_2 and k_3 are

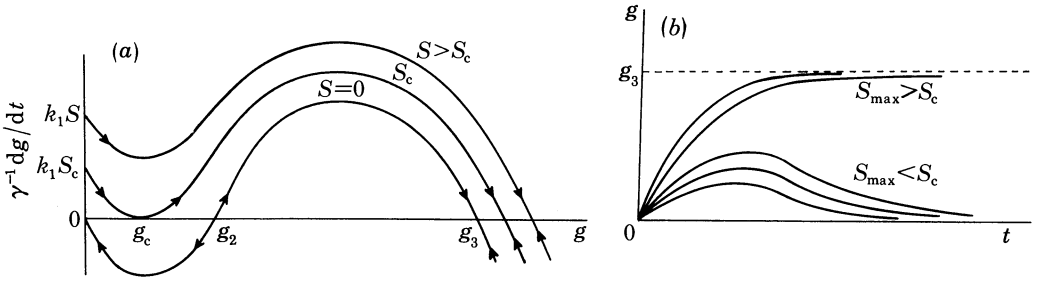

FIGURE 2. (*a*) Illustrative biochemical switch mechanism with typical bistable kinetics from (2): $\gamma^{-1}\mathrm{d}g/\mathrm{d}t = k_1 S + k_2 g^2/(1+g^2) - k_3 g$. The graph shows $\gamma^{-1}\mathrm{d}g/\mathrm{d}t$ against g for given appropriate k_1, k_2, k_3 and several values of S. The critical S_c is defined as shown with two stable steady states for $S < S_c$ and one, $g = g_3$ for $S > S_c$. (*b*) Schematic behaviour of g as a function of time t from (2) (as in (*a*)) for various pulses of S which increase from $S = 0$ to a maximum S_{max} and then decrease to $S = 0$ again. The lowest curve has the smallest S_{max}: successive curves have larger S_{max}. The final state of g, for large time, changes discontinuously from $g = 0$ to $g = g_3$ if S_{max} is greater than the critical S_c.

appropriately ordered, namely $k_2 > 2k_3$ (see the appendix) the plot of $\gamma^{-1}\mathrm{d}g/\mathrm{d}t$ against g exhibits the qualitative S-like shape in figure 2*a*. At a given time, say, $t = 0$, suppose that $g = 0$ everywhere and the morphogen S is released from the wing sources. As S diffuses it activates the gene product since with $S \neq 0$, $\mathrm{d}g/\mathrm{d}t > 0$ and so g increases with time as in figure 2*b*, which are typical curves for g as a function of time for a fixed S. If S never reaches the critical S_c, then as S decreases again to zero so does g after a long time. However, if S reaches S_c, or exceeds it to say $S = S_1$ in figure 2*a*, for a sufficient time, then g can increase sufficiently so that it tends to the local steady-state equivalent to g_3 where $\mathrm{d}g/\mathrm{d}t = 0$ for that value of S. Now since S, governed by (1), eventually tends to zero again, the kinetics curve in figure 2*a* returns to that with $S = 0$. However, now the steady state is $g = g_3$, whereas before it was $g = 0$; a switch has thus been effected. The stable steady states for $S = 0$ are $g = 0$ and $g = g_3$, with $g = g_2$ unstable (see the appendix): stability and instability are indicated respectively by arrows towards and away from the steady state. It is clear that the detailed kinetics of (2) are not critical as long as they exhibit the threshold characteristics illustrated in figure 2.

We can now see how this mechanism, namely the coupling of (1) and (2), in which a finite amount of morphogen S is released from A and P in figure 1*c*, can generate a spatial pattern in gene product (or colour-specific enzyme). The two equations have to be solved simultaneously. The morphogen diffuses and decays as it spreads across the integument of the wing, and as it does so it activates the gene G to produce g. If over a region of the wing $S > S_c$, then g may increase sufficiently from $g = 0$ to move towards g_3 so that as S finally decreases again g continues to move towards g_3 rather than return to $g = 0$. The growth in g, governed by the differential equation (2), is not instantaneous and so the true critical S is actually larger than S_c in figure 2*a*. The coupling of the two processes, diffusion and gene transcription, in effect introduces a time

PHILOSOPHICAL TRANSACTIONS OF THE ROYAL SOCIETY B BIOLOGICAL SCIENCES

lag. Thus as the bolus of morphogen diffuses across the wing, as a quasi-wave (see figure 3*b*), it generates a domain of permanently non-zero values of g, namely g_3, until along some curve on the wing, S decreases sufficiently so that g returns to $g = 0$ with time rather than continue increasing to $g = g_3$. It is suggested that the determination stream of Kühn & von Engelhardt (1933) is a gene or enzyme activating morphogen diffusion-wave such as has been described and that S comes from a zone of polarizing activity.

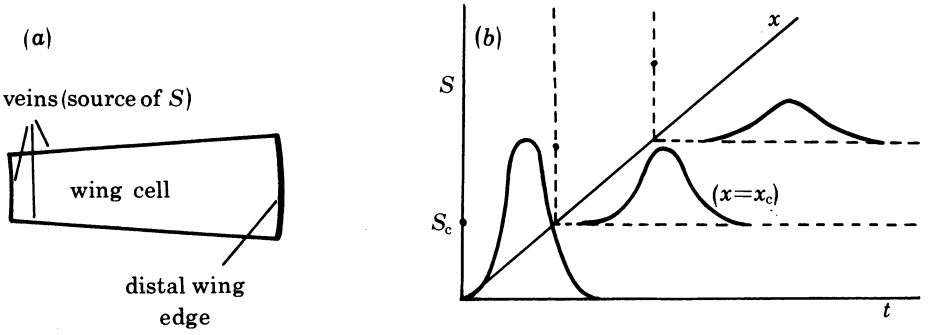

FIGURE 3. (*a*) Idealized representation of a typical wing cell such as those bounded by the media, cubitus anal veins, the discal cell (figure 1*a*) and the distal wing edge. In dependent patterns the veins are considered the source of the gene or cell-specific enzyme activating morphogen. (*b*) Schematic one-dimensional solution for the morphogen S from (1) (see appendix) as a function of time t and distance x, measured perpendicularly from a vein. This quasi-wave of S activates the switch mechanism of figure 2*a* and thus generates a spatial pattern in g. Approximately for $x < x_c$, the position where $S_{max} = S_c$, g tends to $g = g_3$ and for $x > x_c$, g tends to $g = 0$ for large time.

In § 3 I present some numerical results obtained from the model mechanism, compare relevant cases with the microcautery experiments on *Ephestia* (Kühn & von Engelhardt 1933) and *Lymantria dispar* (Henke 1948) and demonstrate some geometry and scale effects on the spatial patterns obtained.

Consider now dependent patterns in which pigment is restricted to the vicinity of the veins. The above model is again a possible mechanism for generating patterns commonly observed. Here I consider the morphogen to be released from the boundary veins of the wing cells. The spatial pattern in g then has a high value of g in the vicinity of the veins and it could be the pre-pattern reflected by the pigment-generating cells. For a given amount of S released, the model shows that the width of the non-zero g-domain on either side of the vein is fixed for given values of the parameters. This is heuristically clear: it is proved mathematically in the appendix. This is consistent with the observation of Schwantwitsch (1924), on nymphalids and certain other families, that although the width of intravenous stripes (in my model the region between the veins where $g = 0$) is species-dependent, the pigmented regions in the vicinity of the veins are the same size. In several species the patterns observed in the discal cell (D in figure 1*a*) reflect the existence of the veins that subsequently atrophy: see figure 7*b*, *c* of the forewing of the female *Troides prattorum* (Papilionidae).

In the model for dependent patterns I consider the wing cell as the unit and idealize it for simplicity, as in figure 3*a*. In the median cells (see figure 1*a*) in particular, the veins are almost parallel. In this case the mathematical problem of a vein source of morphogen is approximately one-dimensional with, say, x distance measured perpendicularly from the vein into the wing cell. The problem for S then has an exact analytical solution (see the appendix). The solution for S as a function of space x and time t is illustrated schematically in figure 3*b*. If $x = x_c$ is the

PHILOSOPHICAL TRANSACTIONS OF THE ROYAL SOCIETY B BIOLOGICAL SCIENCES

distance from the vein ($x = 0$) at which the maximum S is S_c, then from the above discussion we see that this is the maximum possible distance of the non-zero gene product region and, from the model's implication, of the pigmented area. If $S = S_c$ I show in the appendix that x_c, in dimensional terms, is the unique solution of the equation (namely (A 10))

$$z + \ln[2\pi(z-1)S_c/S_0] = 0, \quad x_c = (D/K)^{\frac{1}{2}}(z^2-1)^{\frac{1}{2}}, \tag{3}$$

where S_0 is the amount of morphogen released per unit length of vein. With $D/(\mathrm{cm^2\,s^{-1}})$ and $K/\mathrm{s^{-1}}$, x_c is in centimetres. Note that the distance depends only on the parameters and *not* the scale, which, from observations, is the point noted by Schwantwitsch (1924). It will of course vary from species to species since D and K do. Note that when the systems (1) and (2) are coupled, the non-zero g-region will not move out as far as x_c and so it is not the exact maximum value. The larger γ is in (2), the more accurate it is. However, the dependence of the size of the pigmented area on the various parameters is the same as given by x_c from (3). Since $x_c \propto D^{\frac{1}{2}}$ the appropriate variation in size of the pigmented region should be temperature-dependent accordingly.

Some numerical results from the model are presented in § 3 and, to support my hypothesis, compared with wing pattern examples from various butterflies that exhibit such dependent patterns.

3. Central symmetry and dependent patterns: scale and geometry effects; comparison with observations and experiments

As described above, I shall consider here the central symmetry patterns to be generated by a determination stream emanating from morphogen sources at the wing edges, as in figure 1*b*, *c*. I argued that a morphogen 'wave' progresses across the wing until the morphogen level S has decayed to a critical concentration S_c, at which point the activation kinetics can generate a permanent non-zero product level. I shall now relate the spatial boundary between the two steady-state gene-product levels, the threshold front, with the determination front of Kühn & von Engelhardt (1933). The cells, which reflect the ultimate pigment distribution, are considered to have positional information and react differentially in the vicinity of this threshold front.

Space- and time-dependent solutions of the governing equations (1) and (2) for the morphogen and gene product were found by using a finite difference numerical scheme. There are several parameters that could be varied since there are no estimates available for most of them. I decided that the qualitative behaviour of the pattern formation mechanism and the critical roles played by the geometry and scale could best be highlighted by choosing an appropriate set of values for the parameters in (1) and (2), namely D, k, k_1, k_2 and k_3 and keeping them fixed for *all* of the calculations, the results of which are in figures 4–8. The parameter values did not have to be carefully selected. In all of the central symmetry figures 4–6, a unit amount of morphogen was released at the sources of the determination stream at the middle of the anterior and posterior edges.

Consider first the experiments on *Ephestia kühniella*. Figure 4*a* illustrates a normal wing with typical markings with figure 4*b*, *c* showing the consequences of thermal microcautery (Kühn & von Engelhardt 1933). Figure 4*d* is my idealized normal wing: the lightly shaded region is the residual non-zero gene product left behind the determination wave of morphogen. When a hole, corresponding to thermal cautery, is inserted in the idealized wing and the morphogen

PHILOSOPHICAL TRANSACTIONS OF THE ROYAL SOCIETY B BIOLOGICAL SCIENCES

level is considered to be zero in the hole (that is morphogen diffusing into the hole is lost), results corresponding to the geometry of the experiments are given in figure 4*e*, *f*, which relate respectively to figure 4*b*, *c*. Figure 4*g* is another example with a larger cauterization, while figure 4*h* is of a comparably cauterized wing of *Limantria dispar* after Henke (1948). Figure 4*i* is what the model predicts if cauterization removes the source of morphogen (the zone of polarizing activity) at the posterior edge of the wing: no such experiments appear to have been done to establish where the sources of the determination stream are.

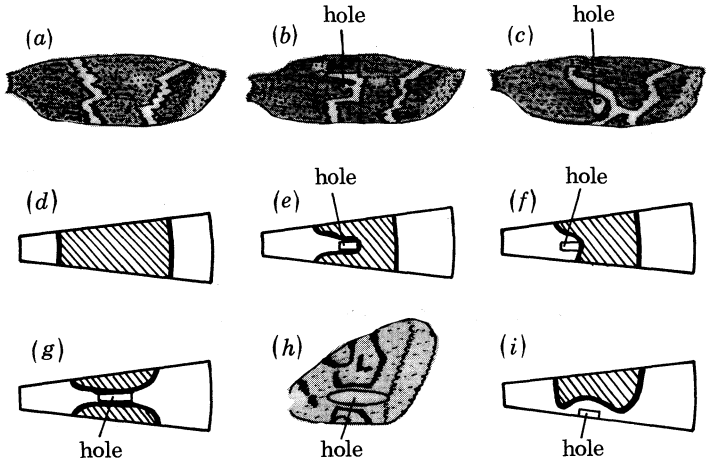

FIGURE 4. Effect of cauterization on the central symmetry pattern. Parts (*a*)–(*c*) are after the results of Kühn & von Engelhardt (1933) on *Ephestia kühniella* (Pyralidae) during the first day after the pupation: (*a*) normal wing, (*b*) and (*c*) cauterized wing with the hole as indicated. (*d*) Idealized model normal wing in which the 'determination stream' has come from sources at the middle of the anterior and posterior wing edges: the hatched region represents a steady-state non-zero gene product. Parts (*e*), (*f*), (*g*) and (*i*) are computed solutions from the model mechanism with cauterized holes as indicated. (*h*) Effect of cauterization, during the first day after pupation, on the cross-bands of the forewing of *Lymantria dispar* (after Henke 1943). Model–experiment comparisons are (*a*)–(*c*), (*b*)–(*e*), (*c*)–(*f*), (*g*)–(*h*). If cauterization removes the determination stream's source (zone of polarizing activity) of morphogen at the posterior edge, the pattern predicted is as shown. Parameter values used in the calculations for equations (A 4) (appendix) for all of (*d*)–(*f*), (*g*) and (*h*): $k_1 = 1.0 = k_3$, $k_2 = 2.1$, $k = 0.1$, $\gamma = 160$ and unit sources of S, $\theta = 0.25$ rad, $r_1 = 1$, $r_2 = 3$.

Even with such a primitive model the variety of patterns that can be generated is large. For the same parameter values for D and the k's, figure 5*a*–*c* illustrate for a *fixed geometry* some of the effects of *scale* on the spatial patterns. These, of course, are as expected heuristically. Central symmetry patterns are particularly common in moth wings. Figure 5*d*, *e* shows just two such examples, namely the chocolate chip (*Psodos coracina*) and black mountain (*Clostera curtula*) moths respectively, similar to figure 5*a*, *b*.

The effect of geometry is also important. With circular sectors some geometric effects are illustrated in figure 6 by simply varying the angle subtended by the anterior–posterior wing edges. Again these are the patterns to be expected when morphogen sources are situated as described above. With wing shapes of less regular geometry, the patterns are more diverse.

Now consider the model as it might apply to dependent patterns in which the veins are the uniform source of the morphogen. Here I consider the model as operating on a single wing 'cell', typically figure 3*a*. I used the same parameter values as before for D and the k's, but now in place of unit sources at specific points I took a uniform source ρ of morphogen along the proximal–distal veins and $n\rho$ along the anterior–posterior vein. I have in mind a typical median

PHILOSOPHICAL TRANSACTIONS OF THE ROYAL SOCIETY B BIOLOGICAL SCIENCES

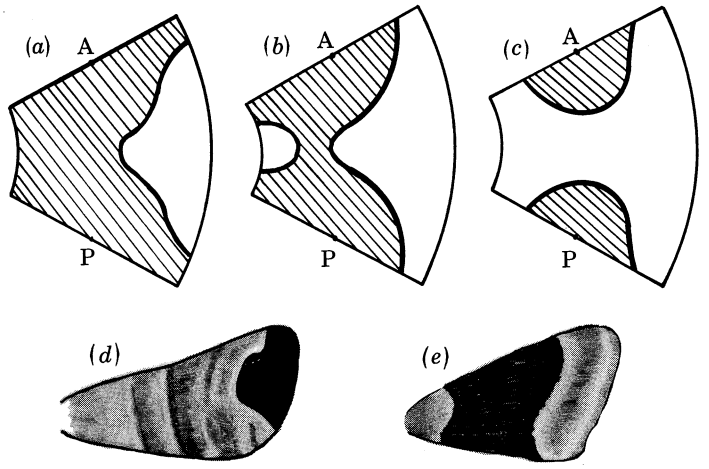

FIGURE 5. Simple effects of scale on spatial patterns. Morphogen S is released from sources A and P. Parts (*a*)–(*c*) illustrate solution patterns with the same set of parameter values ($D = 1$, $k_1 = 1.0 = k_3$, $k_2 = 2.1$, $k = 0.1$, $r_1 = 1$, $r_2 = 3$) in the model mechanism (1) and (2) for different domain sizes: $\theta = 1{\cdot}0$ rad; (*a*) $\gamma = 2$; (*b*) $\gamma = 6$; (*c*) $\gamma = 40$. A wing with $\gamma = \gamma_2$ ($>\gamma_1$) has linear dimensions $\sqrt{(\gamma_2/\gamma_1)}$ larger than that with $\gamma = \gamma_1$. The shaded region represents non-zero gene product. (*d*) *Psodos coracina* (Ennominae) and (*e*) *Clostera curtula* (Notodontidae) are examples of two moth wings, the patterns of which are not uncommon.

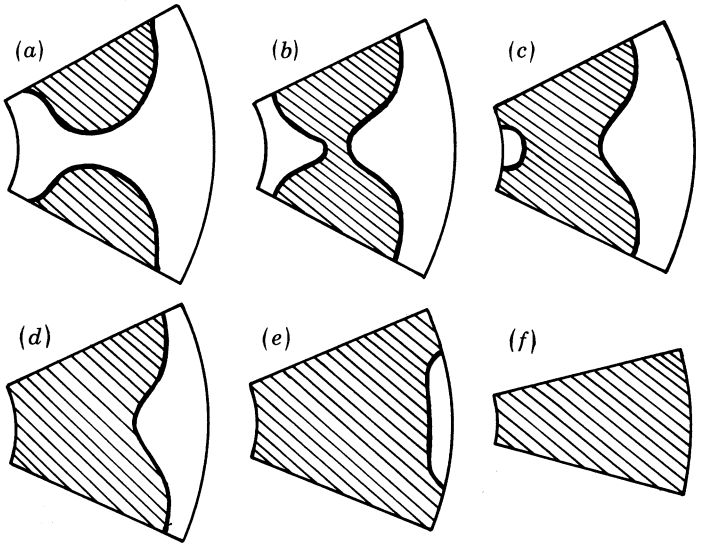

FIGURE 6. Simple effects of geometry on spatial patterns. Morphogen is released as for the calculations in figure 5 with the same parameter values ($D = 1$, $k_1 = 1.0 = k_3$, $k_2 = 2.1$, $k = 0.1$, $r_1 = 1$, $r_2 = 3$) for all calculations from the model mechanism (1) and (2). Here $\gamma = 10$ for all cases, but the angle θ of the sector is varied: (*a*) $\theta = 1.0$ rad, (*b*) $\theta = 0.975$, (*c*) $\theta = 0.95$, (*d*) $\theta = 0.9$, (*e*) $\theta = 0.8$ and (*f*) $\theta = 0.5$.

wing cell and part of the discal vein at the proximal end of the cell: see figure 1*a*. I assume, as before, that there are zero flux boundary conditions for S after the bolus of morphogen has been released. Figure 7 illustrates a typical example of the computed solutions with figure 7*a*, *d* the cell patterns, figure 7*b*, *e* the approximate resulting wing patterns generated and figure 7*c*, *f* specific, but typical, examples of the forewing of *Troides hypolitus* and *T. haliphron* respectively. Such dependent patterns are quite common in the Papilionidae.

Figure 8*a*, *b* shows schematic solutions from (3) on the assumption that the veins are approxi-

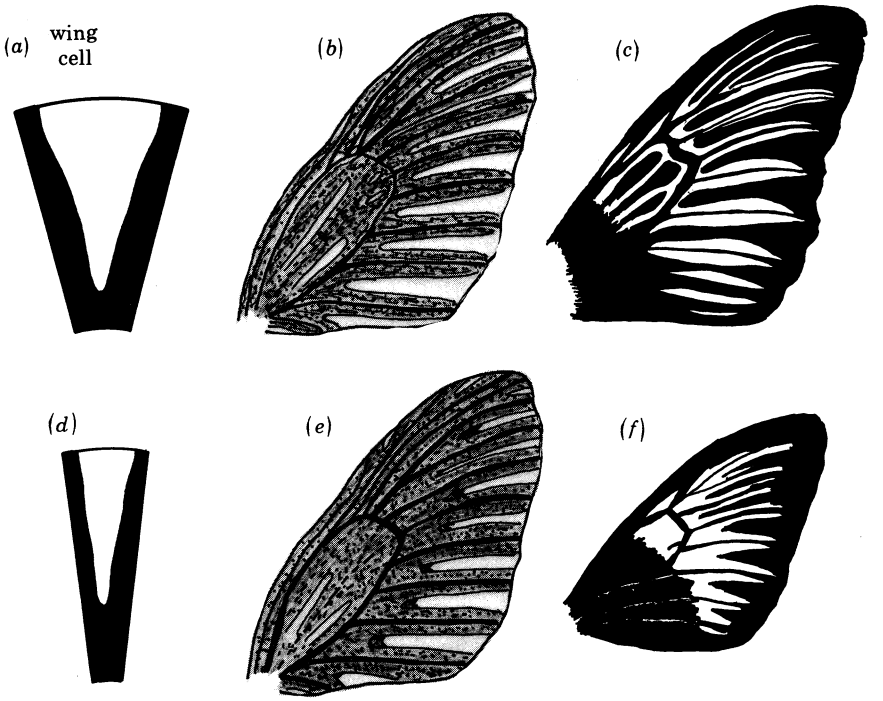

FIGURE 7. Dependent patterns. (*a*), (*d*) Computed patterns from the model mechanism (1) and (2) for a wing cell with parameter values $k_1 = 1.0 = k_3, k_2 = 2.1, D = 1, \gamma = 250$, morphogen source strength in proximal–distal veins (*a*) $\rho = 0.075$, (*d*) $\rho = 0.015$, and $n\rho = 0$ on the cross veins. (*b*), (*e*) Schematic predicted pattern from the wing cell patterns in (*a*), (*d*) applied to the generalized wing of figure 1*a*: shaded regions have a non-zero gene product. (*c*), (*f*) Dependent patterns on the forewing of two Papilionidae: (*c*) *Troides hypolitus*, (*f*) *Troides haliphron*.

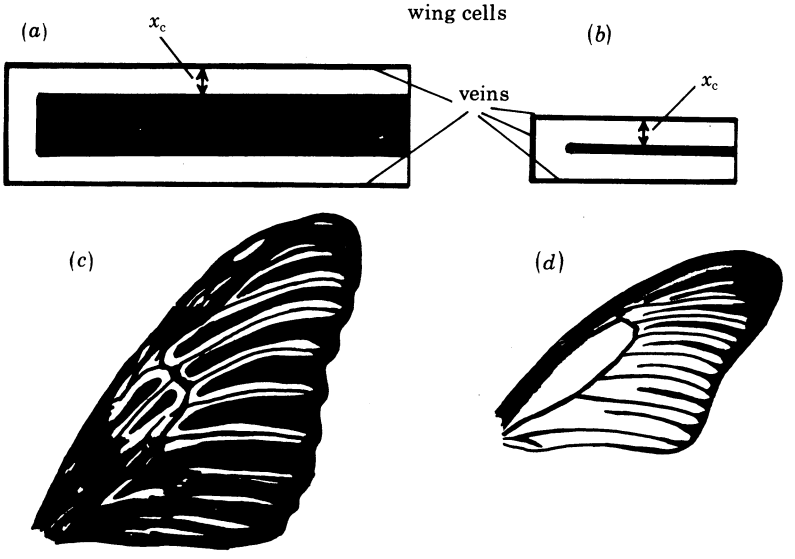

FIGURE 8. (*a*), (*b*) Idealized wing cells from the analytical solution (3) illustrating the effect of scale. The pattern (unshaded) width is fixed for given parameter values. (*c*), (*d*) Dependent patterns from two Papilionidae: (*c*) *Troides prattorum* and (*d*) *Iterus zalmixis*.

PHILOSOPHICAL TRANSACTIONS OF THE ROYAL SOCIETY B BIOLOGICAL SCIENCES

mately parallel. Figure 8*c*, *d* shows examples of the forewings of *Troides prattorum* and *Iterus zalmoxis*. Figure 8*a*, *b* illustrates the effect of scale directly. The qualitative behaviour of the analytical solution (3) shows that the distance from the vein of the pigmented pattern depends in a nonlinear way on the parameters and the amount of morphogen released. If these values are fixed, the distance from the vein is independent of scale. That is, the mechanism shows that the *intravenous* strips between pigmented regions vary according to how large the wing cell is, in agreement with the observations of Schwantwitsch (1924): the two sets of results in figure 8 exemplify this.

4. A general pattern formation mechanism for mammalian coat markings

I shall suppose the distribution of one of the critical components in melanogenesis to derive from a reaction–diffusion mechanism. For illustration only I shall consider a specific substrate-inhibition mechanism where an enzyme is immobilized on an artificial membrane on which a substrate (s) and co-substrate (a) react and diffuse. The experimental arrangement (Thomas 1976) results in the model reaction–diffusion mechanism (Murray 1979, 1981) which in non-dimensional form is

$$\left.\begin{aligned} &\partial a/\partial t = f(s,a) + \beta\nabla^2 a, \quad \partial s/\partial t = g(s,a) + \nabla^2 s,\\ &f(s,a) = \gamma\{\alpha(a_0 - a) - \rho F(s,a)\}, \quad g(s,a) = \gamma\{s_0 - s - \rho F(s,a)\},\\ &F(s,a) = sa/(1 + s + Ks^2), \end{aligned}\right\} \tag{4}$$

for the concentrations s and a, which are functions of space and time t; s_0, a_0, α, ρ, K, β and γ are constants. The $f(s,a)$, $g(s,a)$ represent the reaction kinetics, and $\beta\nabla^2 a$ and $\nabla^2 s$ the diffusion terms: ∇^2 is a shorthand form, which in Cartesian coordinates, for example, is $\partial^2/\partial x^2 + \partial^2/\partial y^2$.

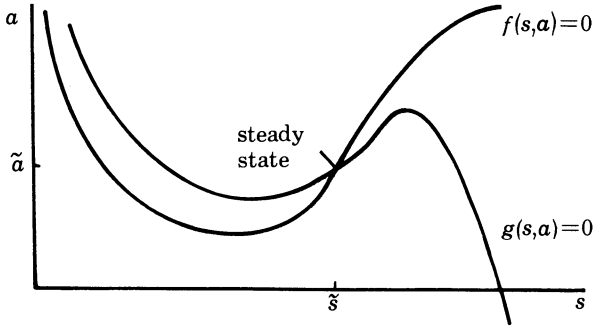

Figure 9. Illustrative rate forms $g = 0$, $f = 0$ for $\mathrm{d}s/\mathrm{d}t = g(s,a)$, $\mathrm{d}a/\mathrm{d}t = f(s,a)$, the reaction kinetics for the model mechanism (equations (4)). The steady states where $\mathrm{d}s/\mathrm{d}t = 0 = \mathrm{d}a/\mathrm{d}t$, are the intersections of $f(s,a) = 0$, $g(s,a) = 0$, namely $(\tilde{s},\tilde{a})$.

The $s_0 - s$ and $a_0 - a$ terms represent flux terms to the reaction surface membrane. $F(s,a)$ is the empirical uptake term which for a given a, for example, is like a Michaelis uptake for small s but which exhibits inhibition for large s with K as the inhibition parameter. Figure 9 shows the general form of the reaction kinetics for the mechanism: the S-like shape of the nullcline $g = 0$ is typical of a substrate-inhibition mechanism. The ratio of the diffusion coefficients on the membrane is β and the scale of the reaction domain is γ, as before. Thus again the size of the domain is proportional to γ (that is, its linear dimensions are proportional to $\sqrt{\gamma}$).

The uniform steady states of the system (4) are the solutions of $f(s,a) = 0 = g(s,a)$ and denoted

by $\tilde{s}$, $\tilde{a}$, that is the intersection of the two curves in figure 9. We are concerned here with the parameter range where only one such solution exists. The forms of f and g in (4) are such that for a range of the inhibition parameter K the steady state $\tilde{s}$, $\tilde{a}$ in figure 9 can be diffusionally driven unstable in the Turing (1952) sense. It can be shown that $\beta > 1$ is necessary, that is the species s and a must diffuse at *different* rates to have a diffusion-driven instability (Murray 1977, 1981).

When the mechanism (4) exhibits diffusional instability it means that the uniform steady state $\tilde{s}$, $\tilde{a}$ is unstable to small *spatial* disturbances. We can consider zero flux boundary conditions for s and a on the reaction–diffusion domain boundary, or alternatively, periodic conditions that reflect the closed surface nature of an embryo's integument. The general features of the patterns obtained are similar.

On a linear basis, that is small variations from the homogeneous steady state, the instability manifests itself in certain unstable modes (solutions) that depend on the scale and geometry of the domain for a given set of parameters in (4). For example, if the domain (integument) is a rectangle $0 \leqslant x \leqslant x_0$, $0 \leqslant y \leqslant y_0$ with x, y Cartesian coordinates and x_0, y_0 constants, small amplitude solutions about $(\tilde{s}, \tilde{a})$ of (4) satisfying the zero flux boundary conditions are of the form

$$e^{\lambda_{mn} t} \cos(n\pi x/x_0) \cos(m\pi y/y_0) \tag{5}$$

for integers m, n. The constants λ_{mn} determine the stability: the specific solution (5) is unstable if m and n are such that $\lambda_{mn} > 0$ since the amplitude grows with time. If $\lambda_{mn} < 0$, it is a stable solution and it tends to zero ($s \to \tilde{s}$, $a \to \tilde{a}$) with time.

If the system (4) with zero flux boundary conditions is diffusionally unstable, then a range of solutions, such as (5), are unstable. For the rectangular domain the integers m, n for such *unstable modes* (and hence spatial pattern generating solutions) can be shown (Murray 1979, 1981) to satisfy

$$\left.\begin{gathered} \gamma(X-Y) < \pi^2(n^2/x_0^2 + m^2/y_0^2) < \gamma(X+Y), \\ X = \frac{1}{2\beta}(\beta + M + \alpha + N), \quad Y = \frac{1}{2\beta}\{(\beta + M - \alpha - N)^2 + 4MN\}^{\frac{1}{2}}, \\ M = \left\{\frac{\beta\rho a(1-Ks^2)}{(1+s+ks^2)^2}\right\}_{\substack{s=\tilde{s} \\ a=\tilde{a}}}, \quad N = \left\{\frac{\rho s}{1+s+Ks^2}\right\}_{\substack{s=\tilde{s} \\ a=\tilde{a}}} \end{gathered}\right\} \tag{6}$$

where

For a fixed set of parameters in the kinetics in (4), the X and Y are simply fixed numbers. The values of X and Y reflect the specific substrate-inhibition reaction kinetics that we are considering and thus remain fixed for given parameter values.

For illustration, if $\alpha = 1.5$, $\rho = 13$, $s_0 = 102$, $a_0 = 77$, $K = 0.1$, $\beta = 5$, then the unstable solutions (5) have integer pairs satisfying, from (6),

$$0.036\gamma < n^2/x_0^2 + m^2/y_0^2 < 0.115\gamma, \tag{7}$$

from which the roles of the *scale* (γ) and *shape* (relative size of x_0 and y_0) can be clearly seen. Suppose $\gamma = 1$, $x_0 = 3$ and $y_0 = 1$; then the only unstable mode (5) has $m = 0$, $n = 1$: this implies a spatial pattern that has half the domain $s > \tilde{s}$ and the other half $s < \tilde{s}$, as in the second case in figure 10. As the domain size (γ) increases, so do the number and type of unstable solutions; in other words, the solutions with all the m, n satisfying (7) with the larger γ. If the domain is long and thin, $x_0 \gg 1$, $y_0 \ll 1$, and so the only unstable modes are those with $n \neq 0$ and $m = 0$ since m^2/y_0^2 with $m \geqslant 1$ lie outside the range allowed by (7). We thus see that if the domain is

PHILOSOPHICAL TRANSACTIONS OF THE ROYAL SOCIETY B BIOLOGICAL SCIENCES

too thin, essentially only one-dimensional modes can be unstable. If the domain is too small, that is γ is small, there are no m and n satisfying (7) and so no spatial pattern can be obtained like the first case in figure 10. On the other hand, if the domain is such that neither x_0 nor y_0 are too small, two-dimensional unstable modes are possible. The first four examples in figure 10 illustrate these points. With periodic conditions in place of zero flux conditions, the same expressions hold, namely (6) and (7) but with $\frac{1}{4}\gamma$ in place of γ.

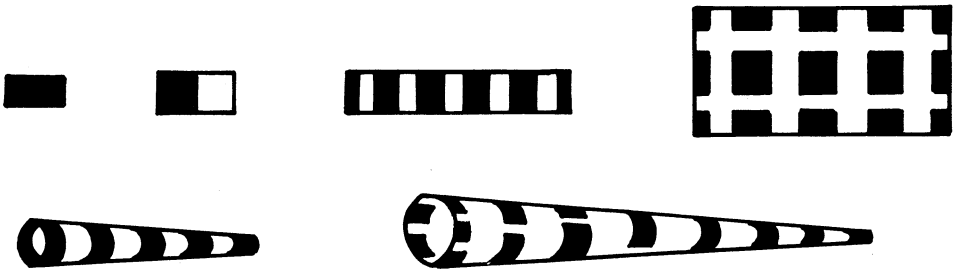

FIGURE 10. Effects of geometry and scale on spatial pattern generated by the model mechanism: simple linear theory predictions with dark–light regions denoting concentration values $s > \tilde{s}/s < \tilde{s}$, where $\tilde{s}$ is the homogeneous steady state.

If we now consider the domain to be the surface of a tapering circular cylinder, the linearly unstable solutions are of the form (Murray 1979, 1981)

$$e^{\lambda_{mn}t}\cos n\theta\cos(m\pi z/l), \quad \gamma(X-Y) < n^2/r^2+m^2\pi^2/l^2 < \gamma(X+Y), \tag{8}$$

where the tapering cylinder is of length l with $0 < z \leqslant l$ and with circumferential variable θ. Here the local radius r of the cylinder is just a parameter. From (8) we see that if r is small, even n^2/r^2 with $n = 1$ is too large to lie in the range (8) and so only $n = 0$, $m \neq 0$ modes in (8) can be unstable. This implies the presence of only stripes, the equivalent of what is shown in the fifth case in figure 10. If, however, r is large enough near one end so that $n \neq 0$ in (8), genuine θ-variations are possible. We thus arrive at the possibility shown in the last of figure 10, namely a gradation from two-dimensional pattern at the thick end to the one-dimensional structure at the thin end.

5. Application of the model mechanism to specific geometries and animals

The analytical solutions described in § 4 are those obtained from a linear theory that gives only the spatial time-dependent behaviour near the onset of the instability. When the system is diffusionally driven unstable, these linearly unstable solutions evolve into a *finite-amplitude steady-state* heterogeneous structure. The full nonlinear mechanism (4) has to be solved by using a finite element numerical method with initial conditions taken to be random variations about the steady state $\tilde{s}$, $\tilde{a}$. Typical computer times for a run are of the order of 1–2 min. I denote, in the following figures from the computed solutions, areas with $s \geqslant \tilde{s}$ by dark shading and $s < \tilde{s}$ without shading. If the domain is too small no pattern is obtained, if it is long but very narrow, only one-dimensional stripes can result, as suggested in § 4. As the domain increases in size, γ increases, more two-dimensional patterns appear.

I considered the mechanism (4) for various two-dimensional geometries for one set of parameters s_0, a_0, α, ρ, K, β, and varied *only* the scale factor γ. Figures 11–14 illustrate the results.

PHILOSOPHICAL TRANSACTIONS OF THE ROYAL SOCIETY B BIOLOGICAL SCIENCES

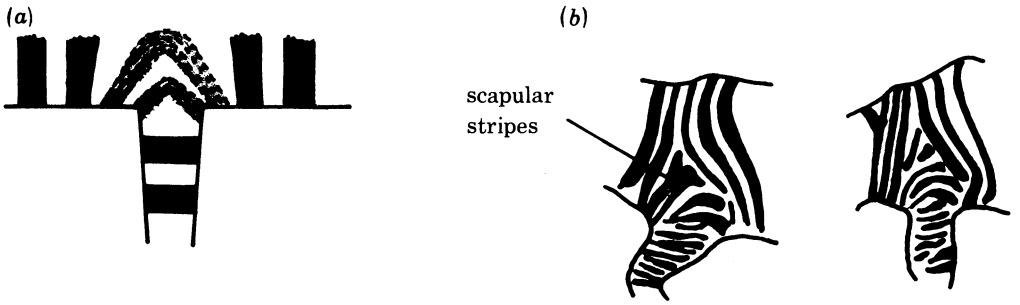

FIGURE 11. (*a*) Predicted spatial pattern from the model mechanism (4) based on a linear theory. (*b*) Typical examples of scapular stripes on the foreleg of zebra (*Equus zebra zebra*).

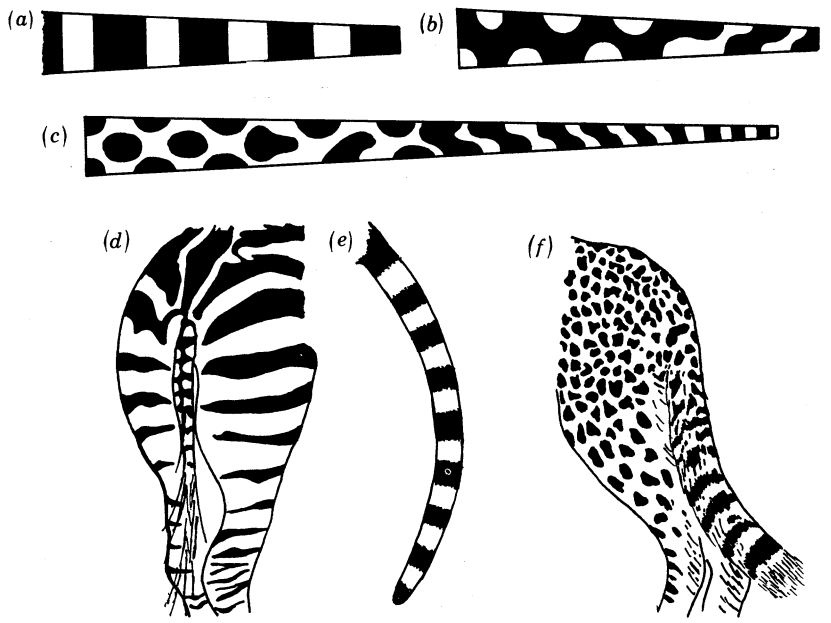

FIGURE 12. Finite amplitude spatial patterns generated by the reaction–diffusion mechanism (4) with parameter values $\alpha = 1.5$, $K = 0.1$, $\rho = 18.5$, $s_0 = 92$, $a_0 = 64$ (steady state $\tilde{s} = 10$, $\tilde{a} = 9$) and diffusion coefficient ratio $\beta = 10$: (*a*) scale factor $\gamma = 9$, (*b*) $\gamma = 15$, (*c*) $\gamma = 25$. Note that for the same geometry, γ is a measure of scale. (*d*)–(*f*) Various animal tail markings: (*d*) Zebra (*Equus burchelli chapmani*) from Willoughby (1974); (*e*) genet (*Genetta genetta*); (*f*) cheetah (*Acinonyx jubatis*).

Figure 11*a* is the schematic model prediction of the pattern that will result when two regions that individually exhibit one-dimensional stripe patterns (as in the third of figure 10) combine as shown. Figure 11*b* shows typical examples of the scapular stripes on the foreleg of zebra.

Figure 12 represents some actual solutions for the finite steady-state structure in s for the planar surface associated with a cylindrical surface that is tapered. As the cylinder size (γ) increases, genuine two-dimensional effects appear. In figure 12*c* we see how the pattern changes from a two-dimensional to a quasi-one-dimensional pattern, a common feature on spotted animals where spots degenerate into stripes at thin extremities, as on tails and legs.† Figure 12*d–f* gives some practical examples from specific animals, typical of their species: figure 12*d* is possibly a parallel for figure 12*b*.

† This indicates a genuine developmental constraint, namely that it is not possible to have a striped animal with a spotted tail: the converse is quite common.

PHILOSOPHICAL TRANSACTIONS OF THE ROYAL SOCIETY B BIOLOGICAL SCIENCES

Figure 13*a* is a sketch of a giraffe embryo 35–45 days old (after Murray 1981): it clearly has the distinctly recognizable giraffe shape, even though the gestation period is about 457 days. We expect the pre-pattern for the coat pattern to be laid down by this time. Figure 13*b* is a sketch of typical neck markings on the reticulated giraffe, with figure 13*c–e* tracings, on approximately the same scale, of trunk spots from the major species. Figure 13*f* shows two patterns computed from the mechanism (4) with the same parameter values as for figure 12. The giraffe is one of the largest animals that still exhibit a spotted pattern.

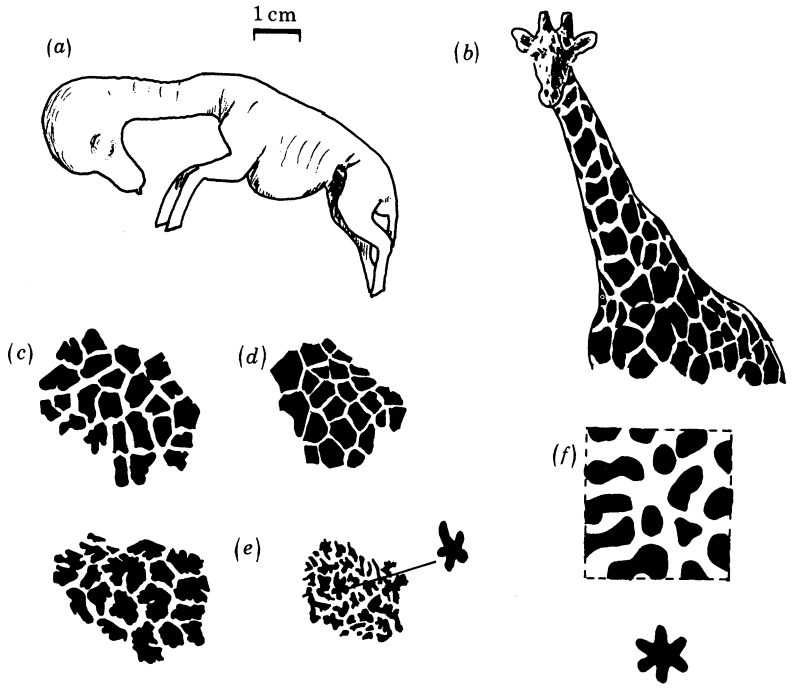

FIGURE 13. (*a*) Giraffe (*Giraffa camelopardalis*): 35- to 45-day embryo (after Murray 1981). (*b*) Typical neck spots on the reticulated giraffe (*Giraffa camelopardalis reticulata*). (*c*)–(*e*) Tracings (after Dagg 1968) of trunk spots (to the same scale) of giraffe, *Giraffa camelopardalis* (*c*) *rothschildi*, (*d*) *reticulata*, (*e*) *tippelskirchi*. (*f*) Spatial patterns obtained from the model mechanism (4) for two different geometries: parameter values as in figure 12.

To show clearly the dramatic effect of scale we considered the shape illustrated in figure 14. It is not suggested that this is a typical shape at the time of pre-pattern formation: it is only a specimen non-simple shape to demonstrate the results. If the size is too small (γ small), no spatial structure can exist. This implies that very small animals can be expected to be uniform in colour; most of them are. As the size increases, spatial patterns can be sustained. For very large domains as in figure 14*f*, the concentration distribution is again almost uniform. This, at first sight unexpected, result is related to the fact that for large γ the linearly unstable solutions of the form (5) have large m and n, which implies a very fine scale of pattern: so small, in fact, that essentially no pattern can be seen. This implies that very large animals are almost uniform in colour, as indeed most are.

Figure 15 gives two striking examples of the half-black, half-white pattern in figure 14*a*, namely the ratel or honey badger (*Mellivora capensis*) and the Valais goat (*Capra aegagrus hircus*).

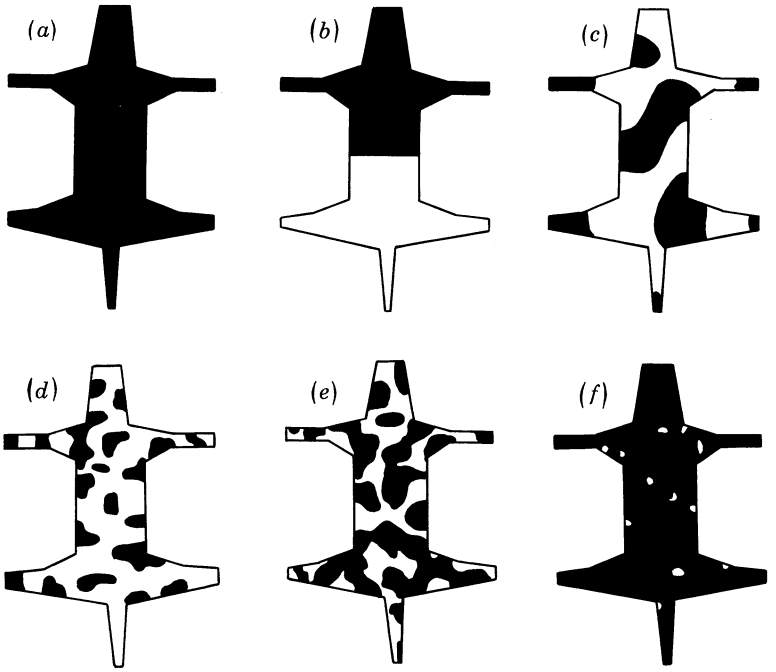

FIGURE 14. Effect of body surface scale on the spatial patterns formed by the reaction–diffusion mechanism (4) for $\alpha = 1.5$, $K = 0.125$, $\rho = 13$, $s_0 = 103$, $a_0 = 77$ (steady state $\tilde{s} = 23$, $\tilde{a} = 24$) and $\beta = 7$. Domain dimension is proportional to $\sqrt{\gamma}$. (*a*) $\gamma < 0.1$; (*b*) $\gamma = 0.5$; (*c*) $\gamma = 250$; (*d*) $\gamma = 1250$; (*e*) $\gamma = 3000$; (*f*) $\gamma = 5000$.

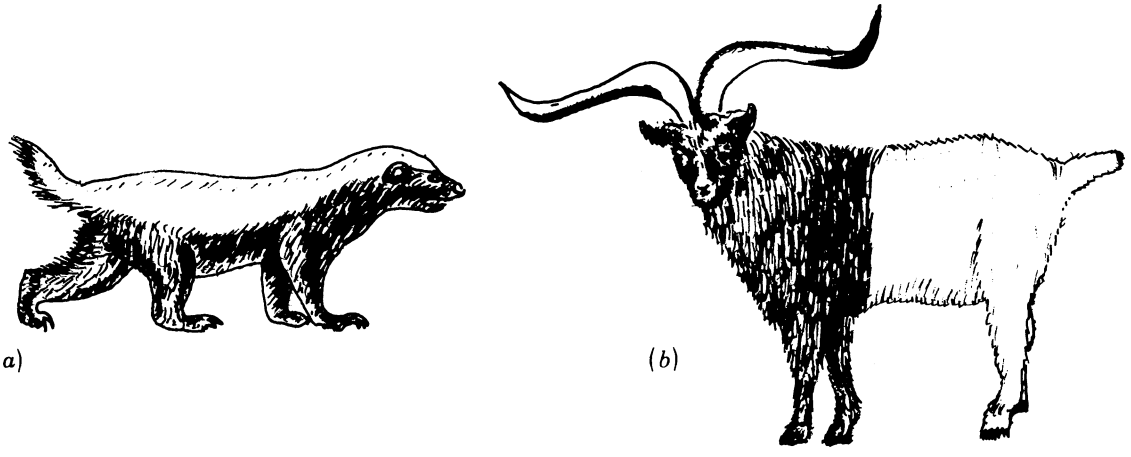

FIGURE 15. Examples of the simplest melanin pattern found in animals: (*a*) ratel or honey badger (*Mellivora capensis*), (*b*) Valais goat (*Capra aegagrus hircus*, after Heráň (1976)).

CONCLUSIONS

Lepidopteran wings

The simple model proposed for generating central symmetry and dependent patterns on wings of Lepidoptera involves a morphogen released from sources (which I consider as zones of polarizing activity) on the wing edges and wing cell veins respectively. The morphogen operates a plausible biochemical switch mechanism to produce a steady-state spatial distribution in a gene product or colour-specific enzyme. This spatial pattern is reflected in the ultimate

pigmented pattern as a result of pigment cells' reacting to the product level laid down. When computed solutions from the model, for the central symmetry patterns, are compared with certain general features in the wings of *Ephestia kühniella* and the experimental work on them (Kühn & von Engelhardt 1933) and *Limantria dispar* (Henke 1948), there is some circumstantial evidence that suggests that such a diffusion model may well be the governing mechanism at least for these species. Evidence from the model and comparison with specific butterflies for dependent patterns, figures 7 and 8, provide further support for diffusion control of pattern.

Experimentally (Kühn & von Engelhardt 1933) a determination stream is evident in the pupal stage shortly after pupation. Dimensions of the field of pattern formation are of the order of several millimetres, which is much larger than any found so far in embryonic fields. One reason for their non-existence in the early stages of embryogenesis is that the development of pattern via diffusion would in general take too long if distances are much larger than a millimetre. In pupal wings, however, this is not so, since pattern can develop over a period of days during which the scale and geometry does not vary very much.

If there is a *combination* of reaction and diffusion, not only can pattern be formed as we saw above, but biochemical messages can also be transmitted: the latter are very much faster than pure diffusion (Murray 1977; Britton & Murray 1979). With butterfly and moth wing patterns, such reaction–diffusion times are too fast unless, of course, they are the means of conveying switch information. Even in the formation of occeli (Nijhout 1980*b*), diffusion times would seem to suffice.

It is most likely that several independent mechanisms are operating, possibly at different stages, to produce the diverse patterns on butterfly wings (Schwantwitsch 1924; Süffert 1925, 1927). It is perhaps reasonable to assume, as a first step, that the number of mechanisms is the same as the number of melanins present. In the case of the nymphalid *Precis coenia* there are four differently coloured melanins (Nijhout 1980*b*).

With the relatively few pattern elements (in comparison with the vast and varied number of patterns that exist) needed in Süffert's (1925, 1927, 1929) groundplan, it seems worth while to explore further the scope of pattern formation possibilities of plausible biochemical diffusion models such as those discussed in this paper. Emphasis should perhaps be with the wing cell as the principal unit (Nijhout 1978). Lepidoptera are particularly suitable for study, since it appears that pattern in the wings is developed comparatively late in development. At the least it would be of interest to study the effect of removal and transplanting of the zones of polarizing activity and of temperature on dependent patterns.

Animal coat markings

A reaction–diffusion mechanism, of which (4) is simply a specific practical example that involves substrate inhibition, exhibits pattern features found in animal coat patterns and these patterns reflect certain general trends. We thus reaffirm the suggestion that a reaction–diffusion mechanism is a possible universal pattern formation mechanism for animal coat markings. The pre-pattern is determined by the size and shape of the integument at the time of laying down. This is probably quite early in gestation. For the zebra, Bard (1977) suggests a time approximately in the 3rd or 4th week. In the model, boundary conditions also play a role but are of less importance: zero flux and periodic conditions give qualitatively similar patterns. The size and shape can only be estimated deductively, since the integument of most foetal specimens is uniform in colour unless just pre-natal or just post-mortem. In the giraffe the rosette patterns

PHILOSOPHICAL TRANSACTIONS OF THE ROYAL SOCIETY B BIOLOGICAL SCIENCES

are seen by about 100 days through gestation, but they quickly disappear *post mortem* (A. J. Hall-Martin, personal communication 1978).

If the pattern formation mechanism is activated (such as by a reduction of the inhibition factor K in (4) by a genetic switch initiating a fast reaction–diffusion wave (Kernevez *et al.* 1978; Britton & Murray 1979)) when the surface is small, uniformity in colour is expected as found in most small animals. On the other hand, if the surface is very large, the mechanism again predicts essentially uniformity, as with the elephant, rhinoceros, and so on.

The first divergence from uniformity in domains long compared with width are stripes. An increase in domain results in patterns such as those on the backs of tigers and zebras. Further increase results in spots with stripes at extremities. For yet larger domains, the spots tend to fill the available space, with the giraffe possibly the largest spotted animal (compare figures 13*f* and 14*e*). Uniformity ultimately again results.

In strictly one-dimensional spatial domains, as discussed by Mimura & Murray (1978*a*, *b*), the fastest growing linear unstable mode predicted the final steady-state structure. In two dimensions this no longer holds: the final steady state depends on the initial conditions. This introduces an important randomness which is a *positive*, or indeed necessary, attribute of the mechanism. The patterns obtained for a given set of parameters but different initial conditions are *qualitatively* similar for a given geometry and scale. This is in keeping with the individuality in animal markings within a species. Since initial conditions always have a random element, individuality of the final pattern is assured.

For the computed patterns obtained from the model mechanism, one set of parameters were taken and *only* the scale, γ, was varied. Even so, the wealth of patterns that can be obtained exhibit certain general features found in pelage markings. It is reasonable to suppose that with other parameter ranges, all of the known patterns on animals can be qualitatively duplicated. With the numerical programme used it is not difficult to seek them, since each run (that is one pattern for a given geometry) takes of the order of 1 min.

The final spatial pattern is determined by the size and geometry of the domain at the time in the embryonic development that the genetic switch, initiating the mechanism, is activated. This time is probably inherited and would suggest that general but not specific markings are inherited. This seems to be so at least for neck markings on the giraffe (Dagg 1968).

The above results are only a few of those found for the mechanism (4), but they nevertheless support a single all-encompassing mechanism for pattern formation for animal coat markings.

Mathematical appendix

Diffusing-morphogen–gene-activation model mechanism

The model mechanism for central symmetry patterns involves the morphogen, with concentration S, released in an amount S_0 at the wing boundaries at A and P in figure 1*c*, the idealized wing geometry under consideration. The morphogen satisfies, from § 2,

$$\frac{\partial S}{\partial t} = D\left(\frac{\partial^2 S}{\partial r^2} + \frac{1}{r}\frac{\partial S}{\partial r} + \frac{1}{r^2}\frac{\partial^2 S}{\partial \theta^2}\right) - KS, \tag{A 1}$$

where r and θ are polar coordinates, t the time, $D/(\mathrm{cm^2\,s^{-1}})$ the diffusion coefficient and $K/\mathrm{s^{-1}}$ the decay relaxation constant. The wing, the diffusion domain for (A 1), is $r_1 \leqslant r \leqslant r_2$, $0 \leqslant \theta \leqslant \theta_0$. S satisfies zero flux boundary conditions and S_0 is released from A ($r = r_A$, $\theta = \theta_0$) and P ($r = r_P$,

$\theta = 0$) as delta functions at $t = 0$. Initially $S = 0$ everywhere. Thus $S(r, \theta, t)$ has initial and boundary conditions for (A 1), as

$$\left.\begin{aligned} S(r, \theta, 0) &= 0 \quad \text{for} \quad r_1 < r < r_2, \quad 0 < \theta < \theta_0; \\ S(r_P, 0, t) &= S_0 \delta(t) = S(r_A, \theta_0, t); \\ \partial S/\partial r &= 0 \quad \text{for} \quad 0 \leqslant \theta \leqslant \theta_0; \quad r = r_1, \quad r = r_2; \\ \partial S/\partial \theta &= 0 \quad \text{for} \quad r_1 \leqslant r \leqslant r_2; \quad \theta = 0, \quad \theta = \theta_0; \end{aligned}\right\} \tag{A 2}$$

where $\delta(t)$ is the Dirac delta function. Equations (A 1) and (A 2) uniquely determine S for all time $t > 0$ and r, θ on the wing. A one-dimensional solution ((A 8) below) is illustrated in figure 3*b*. At any position (r, θ) on the wing in figure 1*c* the morphogen level increases from zero to a maximum value $S_m(r, \theta)$ and then tends to zero again as $t \to \infty$.

Transcription of the gene to give a product or activation of a cell-specific enzyme, which is initially everywhere zero, is governed by a biochemical switch mechanism. The illustrative mechanism from § 2 above is the ordinary differential equation for $g(t)$.

$$\frac{dg}{dt} = K_1 S + \frac{K_2 g^2}{K_4 + g^2} - K_3 g, \quad g(0) = 0, \tag{A 3}$$

where g, the product concentration, is a function of time and space (through S). Equations (A 1)–(A 3) have to be solved simultaneously (although S is independent of g). If the parameters are in an appropriate range this mechanism generates a stable steady-state spatial pattern in g, as explained in § 2.

As always, it is convenient to introduce non-dimensional quantities to isolate the key parameter groupings and indicate relative importance of terms and to make the system units independent. Let l/cm be a standard reference length and a/cm, for example $r_2 - r_1$, a relevant length in the wing of interest. Introduce dimensionless quantities by

$$\left.\begin{aligned} &\gamma = (a/l)^2, \quad S' = S/S_0, \quad r' = r/a, \quad t' = (D/a^2)\, t, \\ &k = Kl^2/D, \quad k_1 = K_1 S_0 l^2/D\sqrt{K_4}, \quad k_2 = K_2 S_0 l^2/D\sqrt{K_4}, \\ &k_3 = K_3 l^2/D, \quad g' = g/\sqrt{K_4}. \end{aligned}\right\} \tag{A 4}$$

I shall now omit the primes in what follows, for algebraic simplicity. The non-dimensional equations (A 1) and (A 3) become, by using (A 4),

$$\left.\begin{aligned} \frac{\partial S}{\partial t} &= \frac{\partial^2 S}{\partial r^2} + \frac{1}{r}\frac{\partial S}{\partial r} + \frac{1}{r^2}\frac{\partial^2 S}{\partial \theta^2} - \gamma k S, \\ \frac{dg}{dt} &= \gamma\left(k_1 S + \frac{k_2 g^2}{1 + g^2} - k_3 g\right) = \gamma f(g), \end{aligned}\right\} \tag{A 5}$$

where $f(g)$ is defined by (A 5).

The reason for introducing γ is for convenience in making scale changes simply. If our 'standard' wing has $a = l$, that is $\gamma = 1$, then for the *same* parameters a similar wing but twice the size has $a = 2l$, that is $\gamma = 4$, but it can be represented by the same-sized figure as for $\gamma = 1$. Thus γ is a direct measure of scale, and is incorporated in the equations.

The initial and boundary conditions (A 2) in non-dimensional form are algebraically the same except that now

$$S(r_P, 0, t) = \delta(t) = S(r_A, \theta_0, t),$$

and all quantities are the dimensionless equivalents from (A 4).

PHILOSOPHICAL TRANSACTIONS OF THE ROYAL SOCIETY B BIOLOGICAL SCIENCES

So that the gene kinetics exhibit a switch mechanism as illustrated in figure 2*a*, the parameters k_1, k_2 and k_3 must satisfy certain relative size conditions. These are that $f(g)$, from (A 5), must have a minimum and maximum for all $S \geqslant 0$ of interest: that is $\mathrm{d}f(g)/\mathrm{d}g = 0$ must have two real roots, which requires that $k_2 > (\sqrt{3})\,k_3$. Also, when $S = 0$, we require as a sufficient condition $f(g) = 0$ to have three real roots, namely $g = 0$, $g = g_2$, $g = g_3$ with $0 < g_2 < g_3$, as in figure 2*a*. This requires that $k_2 > 2k_3$, which covers the previous restriction. Stability of these steady states is obtained from a linearization of the second of (A 5) about the steady states. Writing $f'(g) = \mathrm{d}f(g)/\mathrm{d}g$, we see that a steady-state g_s is stable (unstable) according to whether $f'(g_s) < 0$ ($f'(g_s) > 0$). Thus g_3 is always stable, g_2 unstable and $g = 0$ stable if $S = 0$ and $g = g_1$, the first root when $S > 0$, but $S < S_c$ (in figure 2*a*), is stable. Arrows in figure 2*a* indicate the direction of g as a function of time: the stability or instability is thus indicated.

For the central symmetry patterns, (A 5) were solved numerically by using a finite difference scheme: the computing time for a single case was of the order of 1 min. For illustrative purposes a *fixed* set of parameters k, k_1, k_2, k_3 was chosen and *only* the scale, that is γ, and the geometry were varied. Results are given in § 3.

For comparison with microcautery experiments (Kühn & von Engelhardt 1933), a hole, representing destruction of the cells through which S diffuses, was inserted in the wing, as in figure 4. Since the mechanism is considered to operate during the pupal stage, the morphogen can still diffuse into the hole and is then considered inactive or lost, I chose the mathematical boundary condition $S = 0$ on the hole boundary. More general conditions could easily be used if necessary. Results for this situation are also given in § 3.

For dependent patterns I consider the same mechanism (A 5) with the same boundary conditions (A 2), but now I consider the domain to be an individual wing cell, as in figure 3*a*. The initial conditions, in place of the second and third equation in (A 2), are taken to be

$$S(r, 0, t) = \rho\delta(t) = S(r, \theta_0, t) \quad \text{for} \quad r_1 \leqslant r \leqslant r_2, \tag{A 6}$$

which reflect the fact that the veins are now the source of morphogen S, with ρ simply a parameter that can be varied so as to be able to vary the amount of morphogen released. Again, spatial patterns in g are obtained.

With dependent patterns in wing cells in which the veins are approximately parallel, the diffusing morphogen problem is one-dimensional (at least away from the discal cell vein). The problem, in dimensional form in this case, requires the solution of

$$\partial S/\partial t = D\partial^2 S/\partial x^2 - KS, \quad S(0, t) = S_0\,\delta(t), \tag{A 7}$$

namely

$$S(x, t) = (S_0/4\pi Kt)\exp\{-(x^2/4Dt + Kt)\}, \quad t > 0. \tag{A 8}$$

For a given x the maximum S achieved, $S_{\max}$, is given at time t_m, where $\partial S/\partial t = 0$, which from (A 8) is given by

$$t_m = \frac{1}{2K}\left\{-1 + \left(1 + \frac{Kx^2}{D}\right)^2\right\},$$

which on substituting in (A 8) gives

$$S_{\max}(x) = \{S_0/2\pi(z-1)\}\,\mathrm{e}^{-z}, \quad z = (1 + Kx^2/D)^{\frac{1}{2}}. \tag{A 9}$$

Now from the kinetics mechanism, (A 3), the limiting $S_{\max}$, denoted by S_c, that will effect a switch from $g = 0$ to $g = g_3$ in figure 2*a* can be used in (A 9), by setting $S_{\max} = S_c$, to calculate

PHILOSOPHICAL TRANSACTIONS OF THE ROYAL SOCIETY B BIOLOGICAL SCIENCES

the distance x_c from the vein where $g = g_3$ and hence in our model the domain of a specific pigmentation. That is, x_c is the solution of

$$S_c = \{S_0/2\pi(z_c - 1)\}\, e^{-z_c}, \quad \text{where} \quad x_c = \{(D/K)\,(z_c^2 - 1)\}^{\frac{1}{2}}.$$

An alternative form of the last equation for x_c is

$$z_c + \ln\{2\pi(S_c/S_0)\,(z_c - 1)\} = 0, \quad x_c = \{(D/K)\,(z_c^2 - 1)\}^{\frac{1}{2}}, \tag{A 10}$$

which is the form used in (3) in § 3. Note that z_c and S_c/S_0 are pure numbers with z_c, the solution, a function of S_c/S_0. Then with $D/(\mathrm{cm^2\,s^{-1}})$ and $K/\mathrm{s^{-1}}$ the critical x_c is in centimetres and it depends only on D, K and the ratio S_c/S_0.

A similar finite difference numerical scheme was used for finding the dependent patterns generated by the mechanism. Some results are presented in § 3 above.

References (Murray)

Babloyantz, A. & Hiernaux, J. 1975 Models for cell differentiation and generation of polarity in diffusion-governed morphogenetic fields. *Bull. math. Biol.* **37**, 637–657.

Barde, J. B. L. 1977 A unity underlying the different zebra striping patterns. *J. Zool., Lond.* **183**, 527–539.

Britton, N. F. & Murray, J. D. 1979 Threshold, wave and cell–cell avalanche behaviour in a class of substrate inhibition oscillators. *J. theor. Biol.* **77**, 317–332.

Bunow, B., Kernevez, J.-P., Joly, G. & Thomas, D. 1980 Pattern formation by reaction–diffusion instabilities: application to morphogenesis in *Drosophila*. *J. theor. Biol.* **84**, 629–649.

Crick, F. 1970 Diffusion in embryogenesis. *Nature, Lond.* **225**, 420–422.

Dagg, A. I. 1968 External features of giraffe. *Extr. Mammalia* **32**, 657–669.

Edelstein, B. B. 1972 The dynamics of cellular differentiation and associated pattern formation. *J. theor. Biol.* **37**, 221–243.

French, V., Bryant, P. J. & Bryant, S. V. 1976 Pattern regulation in epimorphic fields. *Science, N.Y.* **193**, 969–981.

Goldschmidt, R. 1920 *Die quantitativen Grundlagen von Vererbung und Artbildung*. Berlin: Springer-Verlag.

Harrison, L. G., Snell, J., Verdi, R., Vogt, D. E., Zeiss, G. D. & Green, B. R. 1980 Hair morphogenesis in *Acetabularia mediterranea*: temperature-dependent spacing and models of morphogen waves. Presented at Workshop on Morphogenesis in *Acetabularia*, Berlin, September.

Henke, K. 1928 Über die Variabilität des Flugelmusters bei *Larentia sordidata* F. und einigen anderen Schmetterlingen. *Z. Morph. Ökol. Tiere* **12**, 240–282.

Henke, K. 1933 Untersuchungen an *Philosamia cynthia* Drury zur Entwicklungsphysiologie des Zeichnungsmusters auf dem Schmetterlingflügel. *Wilhelm Roux Arch. EntwMech. Org.* **128**, 15–107.

Henke, K. 1943 Vergleichende und experimentelle Untersuchungen an *Lymantria* zur Musterbildung auf dem Schmetterlingsflügel. *Nachr. Akad. Wiss. Göttingen, Math.-Physik. Kl.* pp. 1–48.

Henke, K. 1948 Einfache Grundvorgänge in der tierischen Entwicklung. II. *Naturwissenschaften* **35**, 239–246.

Heráň, I. 1976 *Animal colouration: the nature and purpose of colours in invertebrates*. London: Hamlyn.

Kernevez, J.-P., Murray, J. D., Joly, G., Duban, M.-C. & Thomas, D. 1978 Propagation d'onde dans un système à enzyme immobilisée. *C. r. hebd. Séanc. Acad. Sci., Paris* A **287**, 961–964.

Kühn, A. 1926 Über die Änderung des Zeichmungsmusters von Schmetterlingen durch Temperaturreize und das Grundschema der Nymphalidenzeichnung. *Nachr. Ges. Wiss. Göttingen, Math.-Physik. Kl.* pp. 120–141.

Kühn, A. 1936 Über die Determination des Flugelmusters bei *Abraxas grossulariata* L. *Nachr. Ges. Wiss. Göttingen, Math.-Physik. Kl., Nachr. Biol.* **2**, 171–199.

Kühn, A. & von Engelhardt, A. 1933 Über die Determination des Symmetriesystems auf dem Vorderflügel von *Ephestia kühniella* Z. *Wilhelm Roux Arch. EntwMech. Org.* **130**, 660–703.

Lewis, J., Slack, J. M. W. & Wolpert, L. 1977 Thresholds in development. *J. theor. Biol.* **65**, 579–590.

McLaren, A. 1976 *Mammalian chimaeras*. Cambridge University Press.

Mayer, A. G. 1897 On the color and color patterns in moths and butterflies. *Proc. Boston Soc. nat. Hist.* **27**, 243–330.

Meinhardt, H. 1978 Models for ontogenetic development of higher organisms. *Rev. Physiol. Biochem. Pharmac.* **80**, 47–104.

Mimura, M. & Murray, J. D. 1978*a* On a diffusive prey–predator model which exhibits patchiness. *J. theor. Biol.* **75**, 249–262.

Mimura, M. & Murray, J. D. 1978*b* Spatial structures in a model substrate-inhibition reaction–diffusion system. *Z. Naturf.* **33c**, 580–586.

Murray, J. D. 1977 *Nonlinear differential equation models in biology*. Oxford: Clarendon Press.

PHILOSOPHICAL TRANSACTIONS OF THE ROYAL SOCIETY B BIOLOGICAL SCIENCES

Murray, J. D. 1979 A pattern formation mechanism and its application to mammalian coat markings. In '*Vito Volterra*' *Symposium*, Accademia dei Lincei, Rome, December 1979. (Proceedings: Springer-Verlag Lecture Notes in Biomathematics.)
Murray, J. D. 1981 A pre-pattern formation mechanism for animal coat markings. *J. theor. Biol.* **88**, 161–199.
Nicolaus, R. A. 1968 *Melanins*. In *Chemical natural products series* (ed. E. Lederer). Paris: Hermann.
Nijhout, H. F. 1978 Wing pattern formation in Lepidoptera: a model. *J. exp. Zool.* **206**, 119–136.
Nijhout, H. F. 1980*a* Pattern formation in lepidopteran wings: determination of an eyespot. *Devl Biol.* **80**, 267–274.
Nijhout, H. F. 1980*b* Ontogeny of the color pattern on the wings of *Precis coenia* (Lepidoptera: Nymphalidae). *Devl Biol.* **80**, 275–288.
Schwantwitsch, B. N. 1924 On the ground-plan of wing-pattern in nymphalids and certain other families of rhopalocerous Lepidoptera. *Proc. zool. Soc. Lond.* **34**, 509–528.
Schwantwitsch, B. N. 1925 On a remarkable dislocation of the components of the wing-pattern in a Satyride genus *Pierella*. *Entomologist* **58**, 226–269.
Schwantwitsch, B. N. 1929 Two schemes of the wing-pattern of butterflies. *Z. Morph. Ökol. Tiere* **14**, 36–58.
Schwantwitsch, B. N. 1935 On some general principles observed in the evolution of the wing-pattern of palearctic Gatyridae. In *Proc. VIth Congr. Ent.*, pp. 1–8.
Schwartz, V. 1962 Neue Versuche zur Determination des zentralen Symmetriesystems bei *Plodia interpunctella*. *Biol. Zentr.* **81**, 19–44.
Searle, A. G. 1968 *Comparative genetics of coat colour in mammals*. London: Academic Press.
Sibatani, A. 1980 Wing homoeosis in Lepidoptera: a survey. *Devl Biol.* **79**, 1–18.
Smith, J. C. & Wolpert, L. 1981 The increase in width of the chick wing bud following a polarizing region graft and the effect of X-irradiation on pattern formation along the antero-posterior axis. *J. Embryol. exp. Morph.* (In the press.)
Sondhi, K. C. 1963 The biological foundations of animal patterns. *Q. Rev. Biol.* **38**, 289–327.
Süffert, F. 1925 Geheime Gesetzmässigkeiten in der Zeichnung der Schmetterlinge. *Revue Suisse Zool.* **32**, 107–111.
Süffert, F. 1927 Zur vergleichenden Analyse der Schmetterlingszeichnung. *Biol. Zentr.* **47**, 385–413.
Süffert, F. 1929 Morphologische Erscheinungsgruppen in der Flügelzeichnung der Schmetterlinge, insbesondere die Querbindenzeichnung. *Wilhelm Roux Arch. EntwMech. Org.* **120**, 229–283.
Summerbell, D. & Tickle, C. 1977 Pattern formation along the antero-posterior axis of the chick limb bud. In *Vertebrate limb and somite morphogenesis* (ed. D. A. Ede *et al.*), pp. 41–53. Cambridge University Press.
Thomas, D. 1976 Artificial enzyme membranes, transport, memory and oscillatory phenomena. In *Analysis and control of immobilized enzyme systems* (ed. D. Thomas & J.-P. Kernevez), pp. 115–150. New York: Springer-Verlag.
Turing, A. M. 1952 The chemical basis of morphogenesis. *Phil. Trans. R. Soc. Lond.* B, **237**, 37–72.
Willoughby, D. P. 1974 *The empire of Equus*. New York: Barnes & Co.
Wolpert, L. 1971 Positional information and pattern formation. *Curr. Top. devl Biol.* **6**, 183–224.
Wolpert, L. & Hornbruch, A. 1981 Positional signalling along the antero-posterior axis of the chick wing. The effect of multiple polarizing region grafts. (In preparation.)

PHILOSOPHICAL TRANSACTIONS OF THE ROYAL SOCIETY B BIOLOGICAL SCIENCES